# Pannexin 2 is expressed in murine skin and promotes UVB-induced apoptosis of keratinocytes

**Rafael E. Sanchez-Pupo[a], Brooke L. O'Donnell[a], Danielle Johnston[a], Laszlo Gyenis[b], David W. Litchfield[b,c], and Silvia Penuela[a,c,\*]**
[a]Departments of Anatomy and Cell Biology and [b]Biochemistry and [c]Division of Experimental Oncology, Department of Oncology, Schulich School of Medicine and Dentistry, University of Western Ontario, London, ON N6A 5C1, Canada

**ABSTRACT** Pannexins (PANX) are a family of three channel-forming membrane glycoproteins expressed in the skin. Previous studies have focused on the role of PANX1 and PANX3 in the regulation of cellular functions in skin cells while PANX2, the largest member of this protein family, has not been investigated. In the current study, we explored the temporal PANX2 expression in murine skin and found that one *Panx2* splice variant (*Panx2-202*) tends to be more abundant at the protein level and is continuously expressed in developed skin. PANX2 was detected in the suprabasal layers of the mouse epidermis and up-regulated in an in vitro model of rat epidermal keratinocyte differentiation. Furthermore, we show that in apoptotic rat keratinocytes, upon UV light B (UVB)-induced caspase-3/7 activation, ectopically overexpressed PANX2 is cleaved in its C-terminal domain at the D416 residue without increasing the apoptotic rate measured by caspase-3/7 activation. Notably, CRISPR-Cas9 mediated genetic deletion of rat *Panx2* delays but does not impair caspase-3/7 activation and cytotoxicity in UVB-irradiated keratinocytes. We propose that endogenous PANX2 expression in keratinocytes promotes cell death after UVB insult and may contribute to skin homeostasis.

## INTRODUCTION

Pannexins (PANX1, PANX2, PANX3) are channel-forming glycoproteins that participate in paracrine signaling and are expressed in several tissues (Panchin *et al.*, 2000; Penuela *et al.*, 2013). Initial studies showed abundant PANX2 levels in the central nervous system, leading the scientific community to consider that PANX2 expression is restricted. Recent evidence indicates a broader expression and potential functions in other tissues like the skin (Le Vasseur *et al.*, 2014). Only PANX1 and PANX3 orthologues have been characterized in the context of the skin, in the different skin layers and appendages with various localization profiles (Penuela *et al.*, 2007; Celetti *et al.*, 2010). PANX3 remains steadily expressed after skin development (Celetti *et al.*, 2010), while PANX1 has the highest expression levels at early postnatal stages but becomes down-regulated in aged skin (Penuela *et al.*, 2014a). PANX2 expression has also been detected in the skin (Le Vasseur *et al.*, 2014), but its exact distribution profile and regulation have been largely unexplored in this tissue.

Moreover, PANX1 and PANX3 channels are regulated during keratinocyte differentiation and are implicated in regulating proliferation, differentiation, and wound healing (Celetti *et al.*, 2010;

Penuela et al., 2014a; Zhang et al., 2019, 2021). Much less is known regarding PANX2, for which it has been established that it is expressed in brain tissue and participates in regulating neurogenesis (Swayne et al., 2010) and ischemia-induced neurodegeneration (Bargiotas et al., 2011). Besides, PANX2 is down-regulated in lower-grade glioma and was recently shown to influence multiple molecular pathways and immune infiltration in these cancer tumors (Xu et al., 2021).

Interestingly, PANX2 has been identified at the endoplasmic reticulum (ER)–mitochondria interface (Le Vasseur et al., 2019), and it has been suggested to promote cell death. However, the roles of PANX2 seem to be different depending on the type of cell death and the cell insult. For example, although PANX2 has been found down-regulated in gliomas, its overexpression in rat C6 glioma cells reduces their oncogenicity and accelerates staurosporine-induced apoptosis (Lai et al., 2009; Le Vasseur et al., 2019). Furthermore, genetic deletion of Panx2 (along with Panx1) reduces neuronal cell death through necrosis and protects mice from ischemic stroke (Bargiotas et al., 2011). In contrast, it was reported that proinflammatory cytokines reduce PANX2 expression in pancreatic β-cells and increase cytokine-mediated apoptosis, causing severe diabetes in mice (Berchtold et al., 2017). More recently, PANX2 expression was shown to be enriched in prostate cancer cells, negatively regulating a form of cell death known as ferroptosis, where it was implicated in regulating lipid peroxidation and the cell uptake of ferrous iron (Liao et al., 2020). Despite these findings, little is known about the roles that PANX2 might be playing in the skin and whether this pannexin influences cell death of skin cells.

The skin is frequently subjected to damage by UV light, where apoptosis has an important physiological function to maintain homeostasis (Lippens et al., 2005). Notably, PANX2 has been shown to undergo in vitro cleavage by apoptotic caspases-3/7 (Penuela et al., 2013). However, neither the sites for this posttranslational modification nor its occurrence in the cellular context have been confirmed. Considering that PANX2 is present in the skin, it is possible that, in this context, it could undergo cleavage by apoptotic caspases and modulate the UV light B (UVB)-induced apoptosis of these cells.

In the current study, we sought to explore the temporal regulation of PANX2 expression in the developing and mature skin at the protein and transcript levels. Furthermore, we studied PANX2 localization, determined what cell type is primarily expressing PANX2 in the skin, and investigated whether the caspase-mediated cleavage of this pannexin can result from UVB radiation–induced apoptosis as a relevant biological model of cell death in the skin. We hypothesized that PANX2 is cleaved by executioner caspases and promotes the apoptosis of skin cells after UVB insult.

## RESULTS

### Two PANX2 splice variants are expressed in mouse dorsal skin

Owing to the previous role of PANX1 and PANX3 in regulating cellular processes in the skin (e.g., keratinocyte differentiation and wound healing) and the earlier detection of PANX2 in the skin (Le Vasseur et al., 2014), we sought to characterize PANX2 expression in mouse skin. Earlier, we reported (Abitbol et al., 2019) another splice variant (termed as Panx2-202, as mRNA transcript, PANX2-202, as protein variant) that is predicted for the mouse Panx2 gene (Figure 1A; Table 1) and appears in the mouse genome annotation by Ensembl (release 103). PANX2-202 differs in length from the canonical PANX2 encoding a 26-amino-acid (aa) shorter protein of an estimated molecular weight (MW) of ~71.7 kDa.

According to computational annotations, the mouse PANX2-202 (Uniprot identifier: Q6IMP4-2) differs from the canonical PANX2 pro-

tein sequence in the insertion of eight amino acids after position 75 (insertion sequence: "ARVSSLPS") located in the first extracellular loop domain and the replacement of the distal end of the C-terminal region (from 632 to 677) with the "SSSPPSRSREQL" amino acid sequence (Supplemental Figures S1 and S2B). On the basis of these differences, we designed specific PCR primers (Figure 1A) to accurately detect the expression of both isoforms in mouse dorsal skin. Using real-time PCR (qPCR), we detected transcripts of both mouse Panx2 splice variants in the skin at all ages investigated (postnatal day [P] 0, 4 and 4-, 12-week-old skin). At each age investigated, we found no significant differences in mRNA expression levels among Panx2 transcripts when comparing male and female mice (Figure 1B). Interestingly, Panx2-202 was significantly increased only at P0 compared with the canonical variant in male mice, and a similar trend ($p > 0.05$) was observed in female skin, but this difference was not sustained in later ages (P4–12 wk).

At the protein level (Figure 1C), using our rabbit anti–PANX2-CT polyclonal antibody (Penuela et al., 2009; Sanchez-Pupo et al., 2018), we detected multiple immunoreactive bands with one distinctively at the expected molecular size of the smaller PANX2-202 (~70 kDa) variant. This isoform trended more abundant than the canonical PANX2 (expected at ~75 kDa, appearing as a faint band) and was continuously present at all ages investigated. Notably, in 4-wk-old skin, PANX2-202 was transiently increased ($p < 0.05$) compared with other ages (Figure 1, C and D). In addition, immunoblot band profile analysis in 4-wk-old whole-brain lysates showed that the endogenous PANX2 exhibits an immunoreactive band with a higher apparent MW (~85.7 ± 2.3 kDa) and other multiple bands of lower intensity detected at ~75.1 ± 2.1 kDa (Figure 1C, whole-brain lane). In this case, although it cannot be ruled out that the polyclonal nature of the anti-PANX2 antibodies may have led to detection of several immunoreactive species in the brain, the higher MW of the endogenous mouse PANX2 may correspond to the detection of a brain-specific PANX2-palmitoylated isoform previously reported (Swayne et al., 2010), where this particular posttranslational modification was found to modulate differentiation of neurons and tends to alter the migration band of mouse PANX2.

### PANX2 expression is abundant in the epidermis and is likely regulated during the early stages of keratinocyte differentiation

Previously, it has been shown that PANX1 and PANX3 are expressed in the murine epidermis and other skin adnexal structures of the skin (Cowan et al., 2012). Therefore, we sought to localize PANX2 in the skin of C57BL/6N mice using immunofluorescence (IF) staining of skin sections collected at P0, P4, and 4 wk of age. We used three different rabbit polyclonal PANX2 antibodies raised against the intracellular loop (IL-), carboxyl (CT-) or amino (NT) terminal domains (Figure 2; Supplemental Figure S2) of PANX2 (Penuela et al., 2009, 2014b). All the antibodies exhibited abundant intracellular and diffused staining in cells from the suprabasal layers of the skin (stratum spinosum, granulosum, and the cornified layer), suggesting that PANX2 is primarily present in differentiating epidermal keratinocytes (Figure 2) in the skin at P0, P4, and up to 4 wk of age. In addition, we found staining in the cornified layer that may represent nonspecific immunostaining or remnants of PANX2 in that epidermal layer. Besides, a diffused PANX2 staining was also detected in the outer root sheaths of hair follicles and other regions of the dermis (Supplemental Figure S2A).

To further confirm and characterize PANX2 expression in the skin cells, we isolated primary keratinocytes and dermal mouse
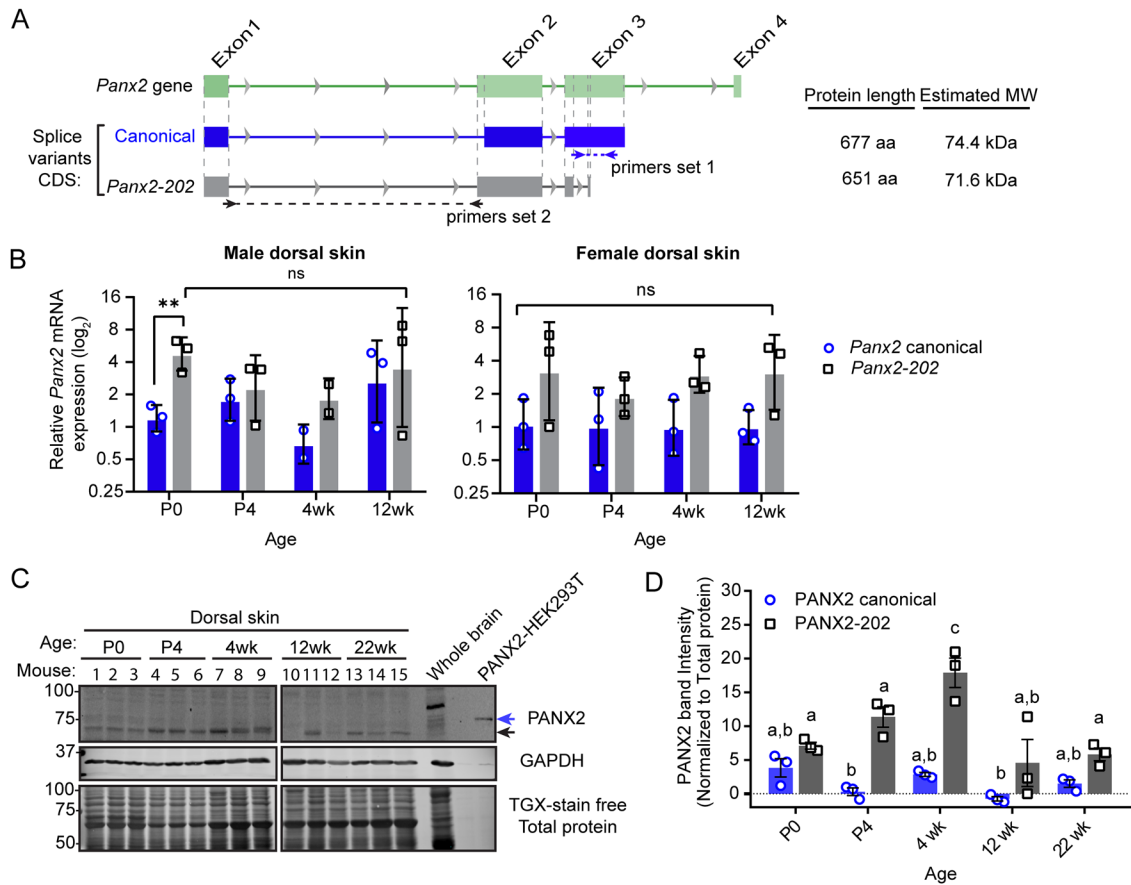
**FIGURE 1:** Transcript and protein levels of PANX2 variants are differentially regulated in mouse dorsal skin. (A) Diagram representing the *Panx2* gene–coding exons in green as per Ensembl (release 103) annotation. Straight lines with gray arrowheads represent the intronic regions of the sequence. Below, blue and gray rectangles depict the coding sequence (CDS) of splice variants vertically aligned with the gene representation at the top. Regions amplified by qPCR primers are shown as dashed lines. Differences in protein length and MW are shown on the right. (B) mRNA expression of each *Panx2* splice variant in male and female dorsal skin. ** denotes $p \leq 0.01$. *Gapdh* was used as the reference gene for normalization. Bars are the geometric mean expression (geomean) $\pm$ SD. (C) WBs showing the canonical PANX2 (~75 kDa, blue arrow) (faint in the skin) and the PANX2-202 splice variant (~70 kDa, black arrow). Migration of skin PANX2 protein bands differed from a major band found in mouse whole brain (4 wk old) (apparent MW of ~89 kDa). Mouse canonical PANX2 (~75 kDa) was overexpressed in HEK293T cells as control (last lane). (D) Densitometric analysis of WB showed a more abundant PANX2-202 that is transiently increased in 4-wk-old mouse skin but restored at previous levels at 12 wk. Two-way analyses of variance (ANOVAs) were used for multiple comparison analysis. Statistical significance (considered when $p < 0.05$) in pairwise comparisons is shown with letters on top of the bars. Means with no letter in common are significantly different.

fibroblasts from skin at P4. Western blots (WBs) with the PANX2-CT rabbit antibody confirmed the presence of the PANX2-202 protein band in both cell types corresponding with the estimated MW (~70 kDa) (Figure 3, A and B). This was consistent with the staining observed in the dermis and epidermis and suggested that PANX2 may not be limited to a single layer of the skin. Because we detected PANX2-202 protein in primary dermal fibroblasts, in vitro experiments were performed to test for changes in *Panx2* mRNA expression upon transforming growth factor beta (TGF-β) induction of fibroblast activation into myofibroblasts. We found that mRNA levels

| Species | Ensembl transcript ID | NCBI RefSeq protein ID | Uniprot ID | Isoform | Length (aa) | MW (Da) |
|---------|----------------------|------------------------|------------|---------|-------------|---------|
| *Homo sapiens* | ENST00000395842.3 | NP_443071.2 | Q96RD6-3 | Canonical | 677 | 74,447 |
| | ENST00000159647.9 | NP_001153772.1 | Q96RD6-1 | Isoform-1 | 643 | 70,641 |
| *Rattus norvegicus* | ENSRNOT00000089707.2 | NP_955441.2 | P60571-1 | Canonical | 674 | 74,434 |
| | ENSRNOT00000089707.1 | — | R9PXY9 | Predicted isoform | 634 | 70,250 |
| *Mus musculus* | ENSMUST00000162424.2 | NP_001002005.2 | Q6IMP4-1 | Canonical | 677 | 74,614 |
| | ENSMUST00000161372.2 | — | Q6IMP4-2 | PANX2-202 | 651 | 71,693 |

**TABLE 1:** Pannexin 2 orthologue information in genomic and protein databases.
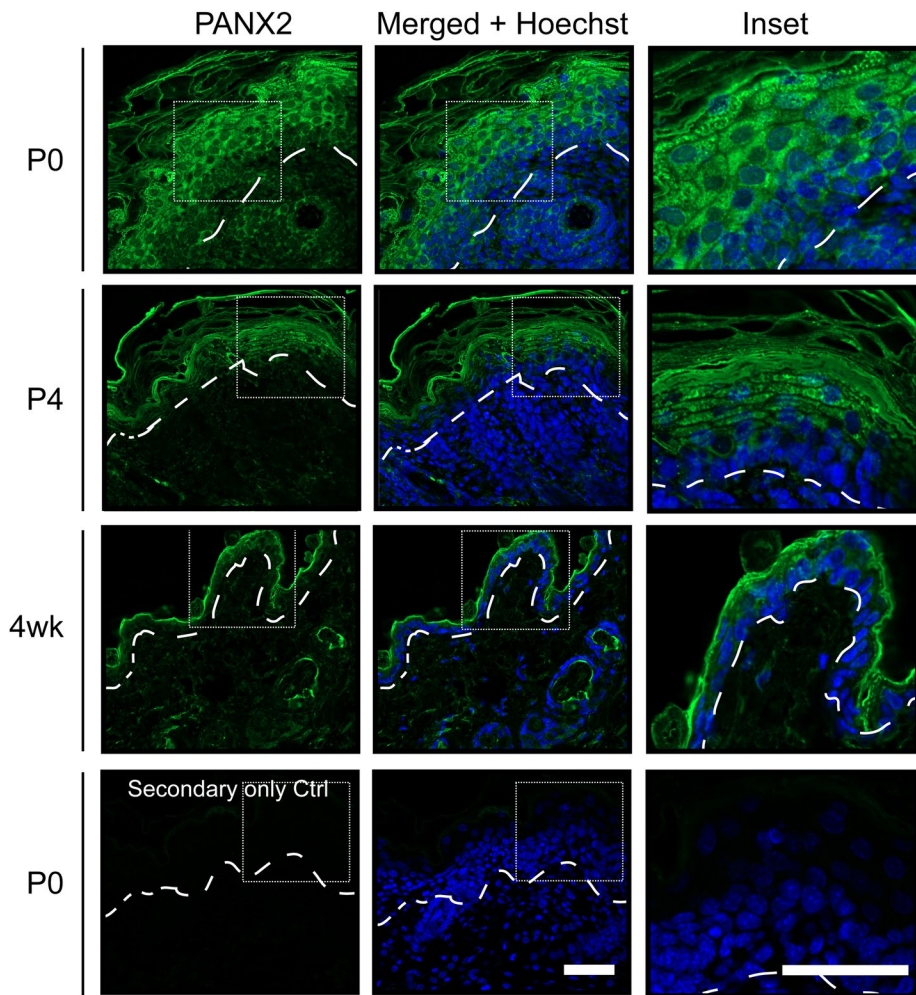
**FIGURE 2:** PANX2 is abundant in the suprabasal layers of the epidermis of mouse dorsal skin. (A) Representative IF micrographs of endogenous PANX2 protein immunostaining (green) in Formalin-fixed sections ($N = 3$) of dorsal skin at P0, 4, and 4 wk. Intense intracellular PANX2 staining with anti–PANX2-CT polyclonal antibody is visualized in cells of the suprabasal layers of the skin. As a control for antibody specificity, sections were stained with the secondary antibody in the absence of the primary antibody (shown as Secondary only Ctrl). Nuclei were stained with Hoechst 33342 (shown in blue), and dashed lines denote the basal membrane dividing the epidermal and dermal layers. Scale bar = 100 μm.

As in vitro differentiation of primary mouse keratinocytes is limited by the finite life span of these primary cells, we also employed an immortalized rat epidermal keratinocyte (REK) cell line (Baden and Kubilus, 1983) to examine changes in the mRNA expression of the rat *Panx2* canonical orthologue during in vitro differentiation. These cells can be grown in traditional media and maintained in culture for long periods while spontaneously initiating differentiation upon reaching confluence when overgrown as cell monolayers (Maher *et al.*, 2005). Therefore, we assayed three conditions: 1) nonconfluent, to resemble a basal-like state, and 72 h–cultured confluent monolayers in the 2) presence or 3) absence of $CaCl_2$ as differentiated stages. We observed that the endogenous rat *Panx2* (canonical) transcript was 3.4-fold significantly up-regulated ($p < 0.01$) after confluency and with a similar effect (1.6-fold, $p < 0.05$) after $CaCl_2$ supplementation compared with the nonconfluent cells (Figure 3F).

While we observed drastic morphologic changes (i.e., cuboidal shape) of the cells under differentiation conditions (not shown), no changes were detected in the transcript expression of the basal marker keratin 14 (*Krt14*). Remarkably, in both confluent and +$CaCl_2$ conditions, we found a significant ($p < 0.05$) increase (189.6- and 194.4-fold, respectively) in transcripts of the rat keratin 10 (*Krt10*), an early differentiation/suprabasal marker. In addition, the late differentiation marker, loricrin (*Lor*), exhibited a 5.3-fold significant ($p < 0.05$) up-regulation, whereas, unexpectedly, involucrin (*Ivl*) was 3.9-fold down-regulated ($p < 0.05$) in confluent versus nonconfluent REK cells. Considering the significant increase in rat *Panx2* transcripts in REK cells, a comparison on the differentiation marker profiles between wild-type (WT) and *Panx2*-deficient cells (later referred to here as REK-PANX2KO cells) was made to assess the effect of the lack of PANX2 during keratinocyte differentiation. However, deletion of rat *Panx2* did not affect the expression profile of *Krt10*, *Flg*, *Ivl*, or *Lor*, which were all significantly increased upon cell confluency and high-$Ca^{2+}$ culture conditions (Supplemental Figure S7). Overall, confluency and calcium supplementation stimulated REK differentiation and increased rat *Panx2* (canonical) mRNA expression in these cells.

### In vitro caspase-3 cleavage of mouse canonical PANX2 C-terminus occurs at D400 and D416

Considering our previous report (Penuela *et al.*, 2014b) on the canonical PANX2 in vitro cleavage by executioner caspases-3/7, we sought to identify the specific sites for caspase-mediated cleavage. Using the webserver Procleave (Li *et al.*, 2020), we obtained a list of putative cleavage sites for caspase-3 (Figure 4A; Table 2). The most likely sites for cleavage were predicted to be located in the canonical PANX2 C-terminal domain, and based on the size of the

of the canonical variant remained unchanged, but *Panx2-202* mRNA was significantly down-regulated after TGF-β treatment (Supplemental Figure S3). On the other hand, as the PANX2 staining was more prevalent in the suprabasal layers of the epidermis, we sought to verify whether PANX2 levels were regulated by early differentiation in keratinocytes. In the epidermis, keratinocytes detach from the basement membrane and occupy the suprabasal layers to undergo terminal differentiation ending in cornification, a specialized cell death process different from apoptosis (Candi *et al.*, 2016). Thus, we tested a commonly used model of in vitro differentiation based on the culturing of primary mouse keratinocytes with increased levels of $CaCl_2$ (Borowiec *et al.*, 2013). However, the increased $Ca^{2+}$ concentration in the culture medium did not markedly alter either the protein levels of PANX2-202 (Figure 3, C and D) nor the expression of both *Panx2* mRNA splice variants. Nevertheless, there was a significant increase in expression of suprabasal/differentiation markers keratin 10 (*Krt10*) and loricrin (*Lor*), indicating early stages of keratinocyte differentiation (Figure 3E).

predicted fragment reported previously (Penuela *et al.*, 2014b), we selected D400 and D416 for site-directed mutagenesis to replace the aspartic residues for alanine (D→A) and generate putative caspase-3/7 cleavage–resistant mouse PANX2 mutants (PANX2[D400A], PANX2[D416A], and PANX2[D400A/D416A]) for validation purposes.

Similar to the methodology used in Penuela *et al.* (2014b), we performed in vitro incubation of immunoprecipitated mouse PANX2 (canonical) with purified active caspase-3 (see Figure 4, B and C) to detect the remaining N-terminal PANX2 fragments after cleavage. In these experiments, caspase-3 cleavage of canonical mouse PANX2 resulted in the loss of immunoreactivity of the band corresponding to the full-length protein (~75 kDa) (Figure 4, D and E). Three major N-terminal PANX2 fragments were identified by WB with apparent MW of 48, 46, and 30 kDa, respectively, as determined by analysis of the lane profiles (Figure 4E; Supplemental Figure S4A). For all the caspase-3–treated groups (canonical mouse PANX2 WT and mutants), a common ~30 kDa protein band was detected, which corresponded with a putative cleavage product if PANX2 caspase cleavage were to occur at D266 (Figure 4, A, C, and E, and Supplemental Figure S4, B–E). In contrast, caspase-3–cleaved mutants PANX2[D400A] and PANX2[D416A] showed the absence of the bands corresponding to each expected N-terminal cleavage product of ~46 and ~48 kDa, respectively (Figure 4E; Supplemental Figure S4, C, D, and F–H). Notably, in the caspase-3–treated (+) lane, the band corresponding to full-length protein is retained for PANX2[D416A] although at a lower intensity, suggesting partial or reduced cleavage efficiency at the amino acid site D400 compared with the D416 site, which was not evident in the PANX2[D400A] mutant. As an experimental control, the specificity of the anti–Panx2-NT antibody was verified using immunoglobulin G (IgG) as a control for the immunoprecipitation (IP), which yielded no background bands in the immunoblots (Figure 4F).

### Mouse canonical PANX2 C-terminus undergoes cleavage at D416 in UVB-induced apoptotic rat keratinocytes

We explored whether caspase cleavage of mouse canonical PANX2 occurs in keratinocytes undergoing apoptosis after UVB exposure. For these studies, due to the availability of the construct, we overexpressed the mouse canonical PANX2 in REK cells. To avoid confounding factors derived from the endogenous rat *Panx2* orthologue expression in these cells, we generated a CRISPR-Cas9–mediated *Panx2* knockout (KO) cell line (REK-PANX2KO). Genotyping and WB confirmed the success of *Panx2*-KO in one of the selected clones (clone 19), indicating a 212-base-pair deletion that encompasses the 1st intron and the 2nd exon of the rat *Panx2* gene verified by Sanger sequencing (unpublished data) (Figure 5, A and B). In WT REK cells, endogenous PANX2 appeared as a faint band (~70 kDa) detected with two commercially available anti-rat PANX2 antibodies that were validated in Wang *et al.* (2009), Swayne *et al.* (2010), and Le Vasseur *et al.* (2014) (Figure 5B).

We hypothesized that the activation of effector caspases-3/7 in UVB-irradiated REK cells induces the cleavage of the mouse canonical PANX2 C-terminus and is likely to promote the programmed cell death process in the cells. Forty-eight hours posttransfection, REK-PANX2KO cells transiently expressing either the mouse canonical PANX2 WT or the PANX2[D400A], PANX2[D416A], or PANX2[D400A/D416A] mutant were exposed to UVB radiation. Full-length mouse PANX2 protein and N-terminal fragments were then immunoprecipitated using the anti–PANX2-NT antibody. WB analysis showed cleaved fragments only in PANX2 WT and PANX2[D400A]-transfected REK-PANX2KO cells, indicating that cleavage of PANX2 in these apoptotic cells occurs only at the C-terminal D416 residue (Figure 5D;

Supplemental Figure S5). Moreover, as expected, ~30 kDa fragments were not observed with any of the constructs, indicating that executioner caspases cannot target the residue D266 that is located in the second extracellular loop of PANX2. Moreover, cleaved caspase-3 was detected only in the post–UVB input lysates, indicating a successful caspase activation and apoptosis after UV irradiation (Figure 5E). Taken together, our results revealed that, in UVB-induced apoptotic keratinocytes, the mouse canonical PANX2 C-terminus undergoes caspase-3/7 cleavage at residue D416.

### PANX2 contributes to UVB-induced apoptosis of REK cells independently of its caspase cleavage

PANX2 has been implicated in different cell death processes (Lai *et al.*, 2009; Bargiotas *et al.*, 2011; Berchtold *et al.*, 2017; Le Vasseur *et al.*, 2019; Liao *et al.*, 2020), from which it seems that any functions during cell death may be dependent on the cell type in question. Based on earlier studies with PANX1 in apoptotic cells (Chekeni *et al.*, 2010), it has been proposed that the irreversible caspase cleavage of PANX1 channels may be detrimental for the cells due to an increased plasma membrane permeability and the repercussion of C-terminal truncation on channel properties and cell death (Sandilos *et al.*, 2012; Engelhardt *et al.*, 2015). To assess whether the PANX2 cleavage contributes to apoptosis in REK cells, we evaluated the effect of genetic deletion of endogenous rat *Panx2*, the rescue with the transient expression of the mouse canonical orthologue (PANX2 WT, 98.2% amino acid sequence identity compared with rat PANX2) and the caspase cleavage–resistant mouse PANX2[D416A] mutant after UVB exposure (Figure 6). We used a green fluorescent DEVD-peptide substrate of caspase-3/7 dye multiplexed with a cell membrane–impermeable cyanine dye (Cytotox Red) to monitor UVB-induced caspase-3/7 activation and cytotoxicity concurrently in an IncuCyte® S3 System live-cell imager.

Our results showed that from 20 to 48 h post–UVB-irradiation, apoptotic caspases were activated in 100% of the cells (Figure 6A, inset). As a quantitative measure for comparing the timing for apoptotic activation between experimental groups, we estimated a parameter (defined herein as $t_{50\%}$, dashed lines in Figure 6A) for the length of time post-UVB required to detect caspase-3/7 activation in ~50% of the cell population. Thus, a delayed caspase activation would correspond to increased values of $t_{50\%}$. Notably, our analysis showed that most groups had significant differences among $t_{50\%}$ ($F_{3,32} = 38.68$, $p < 0.0001$), where REK-PANX2KO cells had a significant delay ($t_{50\%} = 8.7 \pm 0.8$ h, $p < 0.0001$) in caspase activation compared with WT REK cells ($t_{50\%} = 5.9 \pm 0.6$ h) (Figure 6A). Compared to nontransfected REK-PANX2KO cells, overexpression of the mouse canonical PANX2 WT and PANX2[D416A] caspase-resistant mutant elicited a partial rescue increasing the rate of caspase activation ($p < 0.05$) with decreased $t_{50\%}$ of $7.9 \pm 0.3$ h and $7.3 \pm 0.3$ h, respectively (not significant, ns); yet both cases had a $t_{50\%}$ significantly greater ($p < 0.0001$) than that of WT REK cells (Figure 6B). These findings indicated that 1) the genetic deletion of rat *Panx2* (as in REK-PANX2KO cells) delays caspase-3/7 activation and, consequently, the onset of apoptosis, and 2) caspase cleavage of PANX2 (expected in the transfected mouse canonical PANX2 WT) does not affect the timing of executioner caspase activation and thus the apoptosis rate of UVB-irradiated REK cells.

Further analysis showed that at 8 h post-UVB, the % change (compared with 0 h) in caspase-3/7 activation ($F_{3,31} = 40.98$, $p < 0.0001$) was significantly greater ($p < 0.0001$) for WT REK ($89.25 \pm 4.76\%$) compared with the rest of the REK-PANX2KO groups and regardless of their transfection or not with the mouse canonical
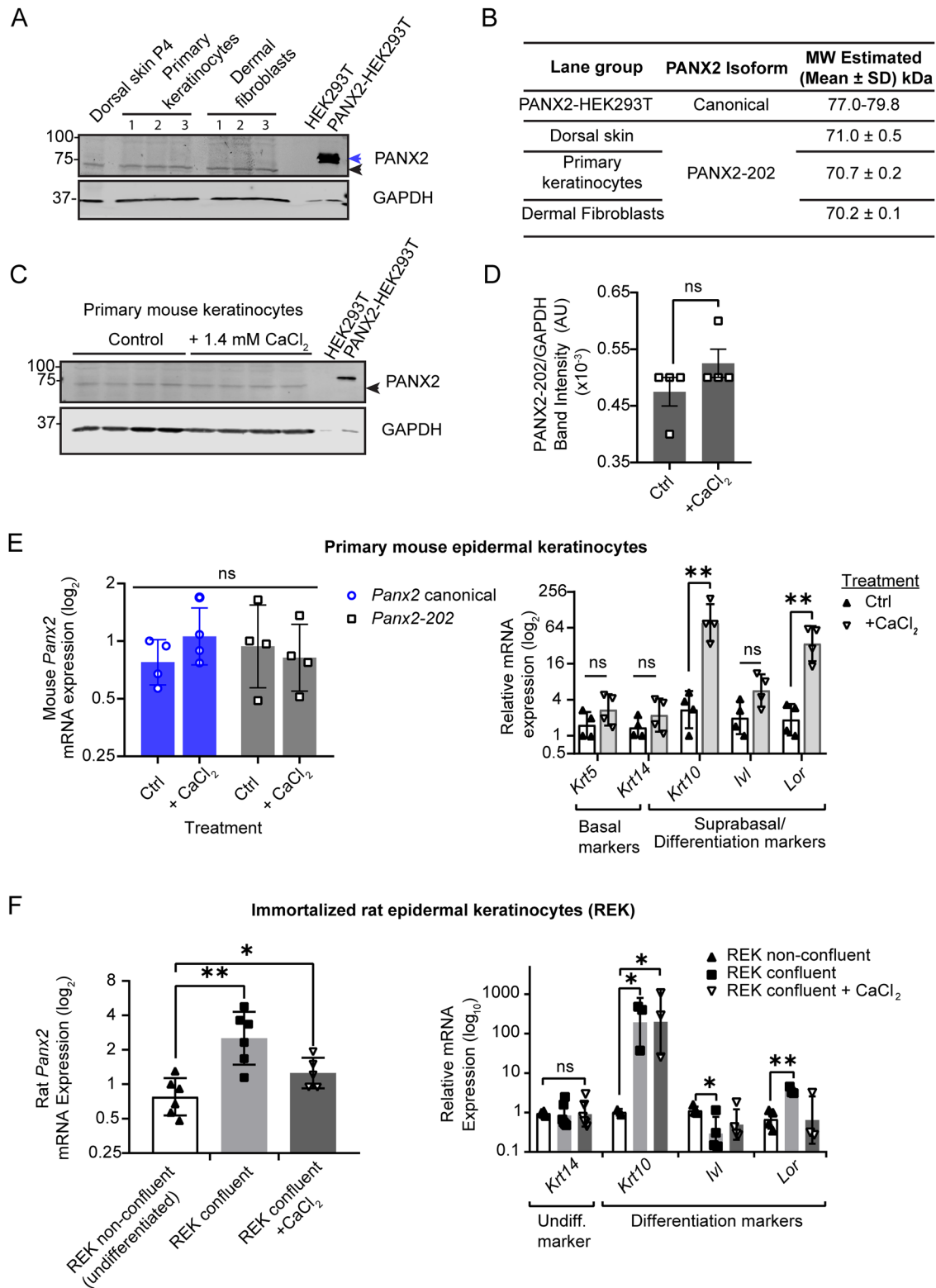
**FIGURE 3:** PANX2 levels are regulated in rat keratinocytes during in vitro CaCl$_2$-induced differentiation. (A, B) Immunoblot used for MW estimation of PANX2 variants detected in primary mouse keratinocytes and dermal fibroblasts. Canonical PANX2 (~75 kDa, blue arrow) and the PANX2-202 splice variant (~70 kDa, black arrow). Numbers indicate different mice. (C–E) Analysis of endogenous PANX2 protein (PANX2-202 splice variant; ~70 kDa, black arrow) and mRNA expression of in vitro CaCl$_2$ differentiation experiments with primary mouse keratinocytes. Four independent primary cell isolations ($N = 4$) were used for the assays. Relative mRNA expression is shown as geometric mean $\pm$ SD. *Gapdh* was used as the reference gene. Unpaired $t$ test was used for statistical analysis of densitometric results in D. ANOVA followed by a Sidak's test was used for multiple comparisons of the log$_2$ (mRNA expression). (F) mRNA expression analysis of *Panx2* rat paralogue in REK cell line in different conditions. One-way ANOVA followed by a
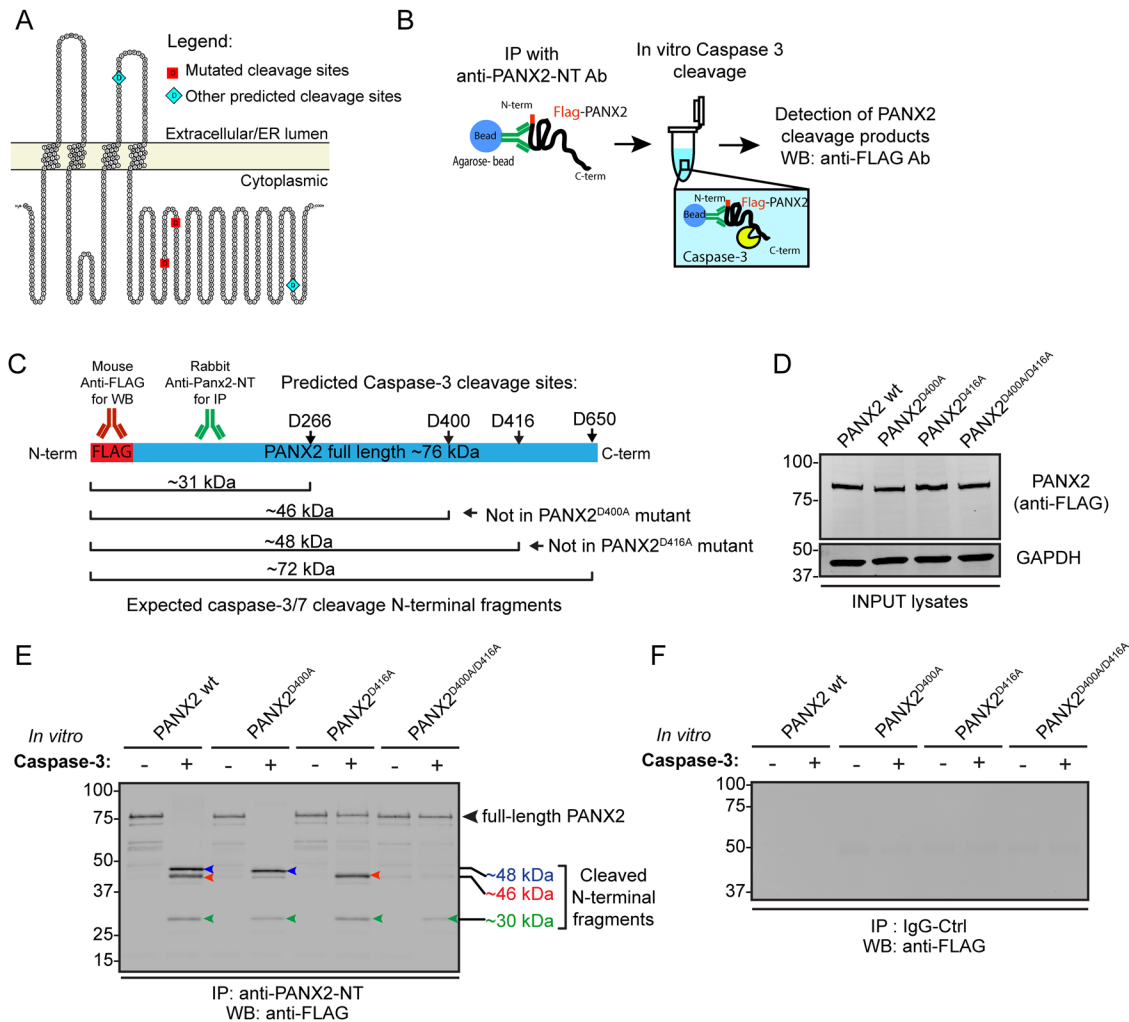
**FIGURE 4:** Canonical mouse PANX2 C-terminus is cleaved by caspase-3 in vitro at D400 and D416. (A) Diagram of the secondary structure of mouse PANX2 showing the putative caspase-cleavage sites (D266, 400, 416, and 650). D400 and D416 were selected for site-directed mutagenesis based on their CT-terminal localization and detectable cleavage products by WB. (B, C) Illustrations depicting expected N-terminal cleavage fragments and the methodology used for IP and detection of the fragments after incubation of PANX2 with purified caspase-3. (D) Immunoblot used as INPUT for IP of protein lysates from overexpressed N-terminal FLAG-tagged PANX2 and caspase-resistant mutants in HEK293T cells. (E) Immunoblot showing IP of full-length PANX2 incubated (+) or not (–) with purified active caspase-3. Protease digestion products were separated simultaneously in the same 10% SDS–PAGE gel and blotted with an anti-FLAG antibody to reveal the N-terminal fragments. Dim bands in the non–caspase treated lanes were considered unrelated degradation products. (F) Immunoblot of controls using IgG for IP. As expected, no background bands confirmed the specificity of the anti–PANX2-NT antibody. Estimation of MW of fragments was performed using densitometric analyses (see Supplemental Figure S4). Results are representative of four independent experiments ($N = 4$).

PANX2 orthologues (WT or D416A). Interestingly, at the 8 h time point, REK-PANX2KO cells overexpressing the noncleavable PANX2$^{D416A}$ mutant (66.52 ± 4.94%) had a significantly higher ($p < 0.05$ and $p < 0.0001$) caspase-3/7 activation than the overexpressing PANX2 WT (54.99 ± 8.43%) and nontransfected (nt) (42.08 ± 14.91%) cells, respectively (Figure 6C). To assess the outcome of the caspase-3/7 activation and apoptotic process across all the time points, we compared the differences ($F_{3, 32} = 12.42$, $p < 0.0001$) in the area under the curve (AUC) from the kinetic caspase activation plots and noticed that regardless of mouse canonical PANX2 WT (or PANX2$^{D416A}$) transfection, the caspase activation rate in REK WT remained significantly higher ($p < 0.05$) compared with that in REK-PANX2KO cells (Figure 6D). However, no differences in the overall caspase-3/7 activation were found between PANX2$^{D416A}$- and

Tukey's test was used for multiple comparisons. Keratinocyte differentiation was assessed by mRNA expression of cytokeratins *Krt5*, *Krt14* for undifferentiated cells; *Krt10*, involucrin (*Ivl*), and loricrin (*Lor*) for late differentiation markers in mouse and rat cells. In each case, mRNA expression was calculated relative to one of the samples of the undifferentiated group control. Unpaired *t* tests were used for comparisons between treatments. Symbols represent different samples or independent experiments with at least $N = 3$. Statistical significance was considered when *$p < 0.05$, **$p < 0.01$.

| Rank | Amino acid position | P4–P4' context | N-terminal fragment size (kDa) | C-terminal fragment size (kDa) | Prediction score | Panx2 domain |
|------|---------------------|-----------------|-------------------------------|-------------------------------|------------------|--------------|
| 1 | 416 | AEPD†GSAE | 47.1 | 27.5 | 0.965 | C-terminus |
| 2 | 266 | ASPD†GPVG | 30.1 | 44.5 | 0.925 | Extracellular loop |
| 3 | 650 | DMGD†LLSI | 71.6 | 3.0 | 0.727 | C-terminus |
| 4 | 400 | TVRD†SGIQ | 45.5 | 29.1 | 0.707 | C-terminus |

†, cleavage site.

**TABLE 2:** Predicted caspase-3/7 cleavage sites in mouse canonical PANX2 according to Procleave.

PANX2KO WTtransfected cells; while, remarkably, the nontransfected REK-PANX2KO group exhibited the lowest ($p < 0.05$) caspase activation. In agreement with the above, these results suggested that in UVB-irradiated REK cells, rat or mouse canonical PANX2 promotes the apoptosis rate (based on the caspase-3/7 activation) regardless of its proteolytic cleavage at D416.
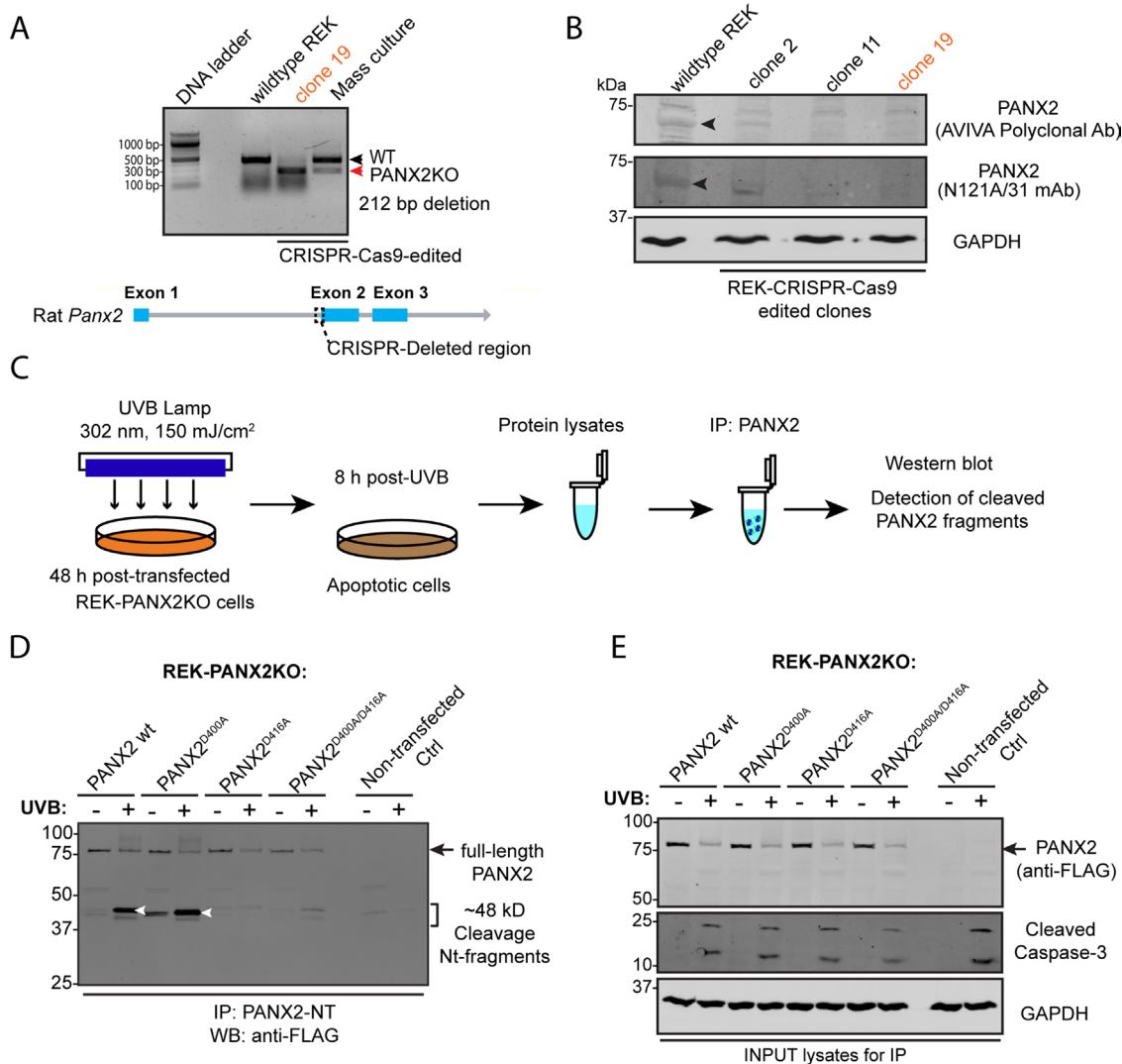


**FIGURE 5:** PANX2 C-terminus is cleaved at D416 during UVB-induced apoptosis of REK cells. (A) Genotyping of rat *Panx2* CRISPR-Cas9 KO REK cells (REK-PANX2KO). PCR of CRISPR-Cas9–targeted region amplified a band with faster migration than WT (red arrow). Sanger sequencing indicated a 212-base-pair deletion encompassing the 1st intron and the 2nd exon of the rat *Panx2* gene. (B) Immunoblot showing the success of PANX2 KO in selected REK-CRISPR-Cas9–edited clones. Endogenous rat PANX2 appears as a ~70 kDa faint band (indicated by arrowhead) no longer visible in the CRISPR-edited REK-PANX2KO cells. (C) Methodology to detect PANX2-cleaved fragments. (D) Immunoblot after IP showing cleavage of canonical PANX2 WT and the mutant PANX2$^{D400A}$ but no PANX2$^{D416A}$ or PANX2$^{D400A/D416A}$ mutants after UVB irradiation. Nontransfected control (Ctrl) lanes indicate nonspecific bands unrelated to PANX2 cleavage. (E) Immunoblot of input lysates showing (cleaved) caspase-3 activation and decreased immunodetection of full-length PANX2 post–UVB irradiation. Results are representative of three independent experiments.

As another measure of cell death, we also assessed changes in the membrane integrity that occurred upon UVB exposure indicating cytotoxicity. After UVB irradiation, a delay in the time of detection in the loss of membrane integrity was found in nontransfected REK-PANX2KO (at ~22–24 h) that was approximately threefold compared with the other groups expressing any PANX2 (~6–8 h) (Figure 6E). Overall, the AUC ($F_{3, 29} = 13.91$, $p < 0.0001$) in the plots of percent change in cytotoxicity was markedly lower ($p < 0.05$) in nontransfected REK-PANX2KO compared with the other groups, while the ectopic expression of mouse canonical PANX2 WT (or PANX2$^{D416A}$ mutant) ultimately rescued the pattern observed in the REK WT cells (Figure 6, E and F). This finding indicates that PANX2 may play a role in influencing membrane disruption or alteration at the later stages of apoptosis in the UVB-irradiated REK cells. Finally, we conducted IF staining and confocal microscopy imaging analysis to rule out any possible effects of the D416A mutation on the subcellular localization of PANX2. The mouse canonical PANX2 WT and its PANX2$^{D416A}$ mutant showed a similar intracellular distribution within REK-PANX2KO cells (Figure 6G) along with the occasional cell membrane and perinuclear localization described in our earlier work (Sanchez-Pupo et al., 2018). In summary, our results suggest that PANX2 promotes UVB-induced apoptotic cell death of keratinocytes, independent of its caspase cleavage.

## DISCUSSION

Alternative splicing has been reported for pannexin genes, but in most cases, the biological relevance of these splicing events remains unknown. Initial work by Baranova et al. (2004) analyzed the human PANX2 sequence, identifying two PANX2 human splice variants, PANX2alt1 and PANX2alt2, with the latter encoding a shorter protein isoform that was speculated to play an unknown regulatory role. In that study, a single mouse Panx2 orthologue was identified by BLAST search, and comparative analysis of the genomic sequence and the transcript expression was validated by in situ hybridizations, but it was limited to the adult murine brain. Here, we have characterized the

**FIGURE 6:** PANX2 promotes UVB-induced cell death of REK cells independently of its caspase-3/7 cleavage. (A–C) Time-course, half-maximal caspase activity ($t_{50\%}$) and time-point analysis of the caspase-3/7 activation. A significant delay in caspase-3/7 activity (increased $t_{50\%}$) was found in REK-PANX2KO compared with WT REK cells. Transient expression of canonical PANX2 WT partially (~50%) rescues caspase activation in REK-PANX2KO cells, with a modest increase when the PANX2$^{D416A}$ mutant is expressed. (D) Overall caspase-3 activation (AUC) was no different between PANX2$^{D416A}$ and PANX2 WT overexpressed in REK-PANX2KO cells. (E) Cytotoxicity time course revealed a delayed and significantly decreased uptake of Cytotox Red Dye by the REK-PANX2KO cells. Similar cytotoxicity onset was found between WT REK and PANX2 WT- and PANX2$^{D416A}$-expressing REK-PANX2KO cells. (F) Overall cytotoxicity (AUC) in PANX2 WT and the PANX2$^{D416A}$ mutant was similar to that observed in REK WT. (G) Representative IF confocal micrographs of REK-PANX2KO cells 48 h posttransfection with PANX2 WT or the PANX2$^{D416A}$ mutant. Similar PANX2 intracellular localization was observed using either the polyclonal PANX2-CT or monoclonal anti-FLAG antibodies. Scale bar = 20 μm. IncuCyte live-imaging caspase-3/7 activation and cytotoxicity data result from 10 technical replicates per group ($n = 10$). One-way ANOVA followed by Tukey's post hoc test was used to compare the means. Statistical significance (considered when $p < 0.05$) is shown with letters on top of the bars. Means with no letter in common are significantly different.

expression of a novel PANX2 isoform (PANX2-202) previously unveiled by us (Abitbol *et al.*, 2019) that bears a MW and partial sequence different from those of the canonical PANX2 found initially in the brain (Panchin *et al.*, 2000; Bruzzone *et al.*, 2003). Furthermore, Abitbol *et al.* (2019) showed that in *Panx1/Panx3* double KO mice, PANX2-202 was expressed in the skin at levels similar to those in WT mice. Our results confirm such findings, although we observed that canonical *Panx2* mRNA transcripts were also present in the mouse skin at all ages investigated.

In the literature, discrepancies in the length and sequence of annotated PANX2 variants exist and are attributed to differences in cloning/sequencing procedures and predictions based on the available genomic sequences (Scemes and Veliskova, 2019). Interestingly, the mouse *Panx2-202* isoform is reported exclusively in the Ensembl database (release 103, as of February 2021) (Table 1) and not in that of the National Center for Biotechnology Information (NCBI). It is important to note that the transcript annotation may vary per genomic database. Ensembl transcripts are automatically annotated based on experimental evidence and are, in most cases, manually curated by the Human and Vertebrate Analysis and Annotation Group (HAVANA) (Aken *et al.*, 2016). However, the NCBI annotations may not match those in Ensembl and include predictions done by a different automated computational analysis (Gnomon method), combining homology searching with ab initio modeling supported by expressed sequence tag (EST) evidence from the current genomic sequences. Most of the studies analyzing mouse PANX2 have worked with the canonical sequence, but it should be noted that the expression of different splice variants may be tissue-specific. Based on the length and sequence, PANX2-202 may have properties (e.g., subcellular localization, channel function, and interaction with binding partners) different from those of canonical PANX2. However, the functional implications of these differences and the consequences of their differential expression remain to be evaluated.

### PANX2 in the skin is up-regulated in differentiated keratinocytes but does not influence their terminal differentiation

We found that PANX2 is present in the suprabasal layers of the skin epidermis and, in contrast to the other pannexins paralogues (Celetti *et al.*, 2010; Cowan *et al.*, 2012; Penuela *et al.*, 2014a), its expression is not drastically affected by the age or sex of the mice. Notably, the PANX2-202 variant trended to be more abundant than the canonical isoform at all ages and sexes assayed. However, transient differences at P0 (at mRNA level in male mice) and at 4 wk old (at the protein level) could indicate an age-specific temporal regulation of PANX2 levels in the skin, yet with unknown biological significance. Nevertheless, the apparent disparity in mRNA and protein expression levels is in agreement with previous findings that mouse *Panx2* transcripts do not correlate with their protein levels (Le Vasseur *et al.*, 2014).

PANX2 seems to have a localization pattern similar to those of PANX1 and PANX3 in the stratum granulosum and spinosum of thin murine skin (Penuela *et al.*, 2007; Celetti *et al.*, 2010; Cowan *et al.*, 2012). In this paper, three different anti-PANX2 polyclonal antibodies were employed for IF, showing an intracellular localization, which correlates with previous observations made by us and others in other cell types and ectopic overexpression systems (Penuela *et al.*, 2009; Wicki-Stordeur *et al.*, 2013; Le Vasseur *et al.*, 2014, 2019; Sanchez-Pupo *et al.*, 2018). However, given that this endogenous labeling was not compared with a true negative control (e.g., *Panx2*-KO tissue), the diffuse staining pattern may arise from other proteins

due to the polyclonal nature of the antibodies, and further confirmation is still warranted.

The level of PANX1 and PANX3 is regulated during keratinocyte differentiation (Celetti *et al.*, 2010; Cowan *et al.*, 2012; Penuela *et al.*, 2014a); therefore, we asked whether PANX2 could be influenced by differentiation in keratinocytes. In primary keratinocytes, PANX2-202 protein was more abundant than the canonical isoform, suggesting that this is the most prominent *Panx2* splice variant in this cell type in culture. Our in vitro differentiation experiments with primary keratinocytes and REK cells showed similar trends with increased mRNA and protein expression of endogenous PANX2 orthologues in differentiated keratinocytes. However, we observed slight differences in the profiles of differentiation markers in primary mouse and immortal keratinocytes, which could be explained partially due to the different nature of the cells, as the mouse-derived keratinocytes were primary cells isolated from newborn mice and REK were an immortalized cell line derived from newborn rat skin (Baden and Kubilus, 1983). Nevertheless, considering the high staining intensity of PANX2 in the stratum spinosum and granulosum of the mouse epidermis and the putative detection of both variants of our antibodies and the trends of increasing protein levels after $Ca^{2+}$-induced keratinocyte in vitro differentiation, we concluded that PANX2 is most likely to be up-regulated during keratinocyte differentiation. Interestingly, the loss of PANX2 in REK-PANX2KO did not impair the terminal differentiation of keratinocytes, indicating that PANX2 is not essential to this process (Supplemental Figure S7). Nonetheless, further work should address whether PANX2 forms functional intracellular channels in keratinocytes and its role during keratinocyte differentiation.

### Canonical PANX2 supports keratinocyte apoptosis independently of its caspase cleavage

Accumulating evidence implicates PANX2 in different cell death processes such as necrosis in neurons, apoptosis in glioma cells, cytokine-induced apoptosis in β-cells, and ferroptosis in prostate cancer cells (Lai *et al.*, 2009; Bargiotas *et al.*, 2011; Berchtold *et al.*, 2017; Le Vasseur *et al.*, 2019; Liao *et al.*, 2020). The skin is often challenged by UV radiation (particularly UVB), causing several skin pathological conditions (Li *et al.*, 2001); therefore, apoptosis constitutes a protective mechanism essential to remove UV-damaged skin cells (e.g., keratinocytes) and avoid the risk of malignant transformation. Keeping in mind that PANX2 could be implicated in cell death, we sought to study the contribution of canonical PANX2 during UVB-induced cell death of keratinocytes. Here, we uncovered for the first time that PANX2 undergoes caspase-mediated cleavage in apoptotic keratinocytes. In continuation of our previous studies (Penuela *et al.*, 2014b), we have identified two sites (D400 and D416) in the mouse canonical PANX2 C-terminus that are targeted in vitro by executioner caspase-3 and demonstrated that in REK cells, at least only one of the predicted sites (D416) undergoes cleavage upon UV irradiation. Notably, genetic deletion of endogenous rat PANX2 delayed but did not prevent REK UVB-induced apoptosis, indicating that PANX2 is not essential but contributes to the apoptotic machinery in these cells. Furthermore, overexpressing canonical mouse PANX2, especially the caspase-resistant mutant PANX2[D416A], accelerated the caspase-3 activation rate and membrane permeability in UVB-irradiated REK-PANX2KO cells. Therefore, we concluded that caspase-mediated cleavage is not needed for the role of PANX2 in the apoptosis of UVB-damaged cells. Nevertheless, these results are in keeping with the proapoptotic function of PANX2 (Le Vasseur *et al.*, 2019).

It is essential to note that despite the high conservation of the canonical PANX2 proteins between both mouse and rat species (98.2% identity), the amino acid sequence of endogenous rat PANX2 has a natural conservative substitution of aspartic acid with glutamate at position 416 (D→E), which is not present in human PANX2 (Supplemental Figure S6). Based on this difference, endogenous rat PANX2 (as in WT REK) is not expected to be cleaved by caspases 3/7. In this respect, our results support our hypothesis that PANX2, but not its caspase-mediated cleavage, functions as a promoter of UVB-induced apoptosis, as it was shown with both PANX2 orthologues. Moreover, regarding the murine PANX2-202 isoform, both cleavage sites at D400 and D416 are still conserved in the amino acid sequence; therefore, we speculate that a similar caspase cleavage is likely to occur (Supplemental Figure S1). However, future work should address whether the PANX2-202 function is affected by caspase cleavage under apoptotic conditions. Remarkably, the PANX2-202 splice variant shares 91% sequence identity with the shorter human variant (isoform-1) (Table 1). We could speculate that such a splice variant may act as the homologue of murine PANX2-202 in human skin. This highlights the possibility of conservation in the expression and regulation of these PANX2 orthologues but has yet to be investigated. To our knowledge, there are no reports of abnormal skin phenotypes in the *Panx*-KO mouse model (Bargiotas *et al.*, 2011, 2012; Dickinson *et al.*, 2016; Berchtold *et al.*, 2017). Nevertheless, considering that PANX2 assists with the death of UV-damaged keratinocytes, skin homeostasis in *Panx2*-KO mice might be compromised after UV exposure or might be more susceptible to UVB-induced skin cancer. Thus, it will be interesting to determine whether *Panx2*-KO mice have defects in skin repair or renewal processes.

In the literature, it has been shown that PANX1 channel permeability is influenced by caspase 3/7 cleavage (Chekeni *et al.*, 2010; Penuela *et al.*, 2014b) but such events are yet to be demonstrated for PANX2. The long C-terminal tail of canonical PANX2 and its difference in sequence from that of PANX1 make it difficult to predict the effect of such cleavage without preliminary evidence of alteration in PANX2 channel function. However, given that caspase-mediated cleavage is not needed for PANX2 to promote the apoptosis of UVB-damaged cells, we could speculate that PANX2 function in this case is likely independent of the caspase cleavage in the C-terminus. Additionally, PANX2 intracellular localization (e.g., ER–mitochondria contact sites [Le Vasseur *et al.*, 2019]) may play a larger role during the apoptotic process that could involve both channel-specific and unspecific properties, but this must be validated by further studies.

In conclusion, this work sheds light on PANX2 regulation in the skin and specifically during two critical processes related to skin homeostasis: keratinocyte differentiation and apoptosis. We demonstrated that the expression of splice variants is a factor to be considered when studying PANX2 in the skin and perhaps in other tissues. This is the first study to identify the caspase-3 cleavage sites in PANX2 and its proapoptotic role in keratinocytes. These novel findings provide a better understanding of the tissue-specific regulation and function of PANX2.

## MATERIALS AND METHODS
### Cell lines, transfection, and culture conditions
Human embryonic kidney (HEK293T CRL-3216) cells were obtained from the American Type Culture Collection (ATCC) (Manassas, VA). The REK immortalized cell line was a kind gift from Dale Laird at Western University and was previously characterized in Baden and Kubilus (1983) Maher *et al.* (2005), and Penuela *et al.* (2014a). Media and most supplements were obtained from GIBCO (Grand Island, NY) and Invitrogen (USA). Unless otherwise stated, cells were grown in DMEM (1×) (GIBCO; REF#12430-054; Grand Island, NY) supplemented with 10% fetal bovine serum (FBS) (Wisent; Cat#080-150; QC, Canada), 1% penicillin–streptomycin (Pen Strep) (GIBCO; REF#15140-122; Grand Island, NY) and maintained at 37°C under humidified 5% $CO_2$–95% air. For in vitro differentiation studies with REK cells, the culture medium was supplemented with calcium chloride at 2.0 mM final concentration for 72 h, or stratified piles of overgrown monolayer cultures were kept for the same length of time. For transient transfections, the cells were transfected using 5 µg of plasmid DNA with Lipofectamine 3000 (Invitrogen; REF#L3000-015; Carlsbad, CA) as per the manufacturer instructions. For apoptosis assays, 24 h posttransfection, cells were split in half for IF staining, with the rest used for Incucyte Live-cell imaging of UVB-induced apoptosis experiments.

### Isolation and culture of mouse epidermal keratinocytes and dermal fibroblasts
The Animal Care Subcommittee of The University of Western Ontario approved all procedures with mice (Protocols 2019-069 and 2019-070). Isolation of primary keratinocytes and dermal fibroblast from neonatal dorsal skin (P4) was performed following the protocols described in Penuela *et al.* (2014a). Primary keratinocytes were cultured in KBM Gold Basal Medium (Lonza; Cat#00192151; Walkersville, MD) supplemented KGM-Gold Keratinocyte SingleQuots (Lonza; Cat#:00192152; Walkersville, MD) at 37°C, 5% $CO_2$. The culture medium was replaced first at 16 h postharvesting and later every 48 h. Keratinocytes were kept for up to 3 wk until they reached 60–70% confluency without any passaging before the experiments. For primary keratinocyte in vitro differentiation, nonconfluent cell monolayers were exposed for 72 h to culture medium supplemented with a final concentration of 1.8 mM $CaCl_2$. Fibroblasts were cultured in DMEM supplemented with 10% FBS and 1% Pen Strep and grown in plates coated with type I rat tail collagen (Corning; REF#354236; Bedford, MA) until the cells reached 70–80% confluency. Cultures of primary dermal fibroblasts were passaged only for a maximum of three times, and visual inspection of a spindle-shaped morphology was continuously assessed before the experiments. Fibroblast stimulation with TGF-β was performed as indicated in Penuela *et al.* (2014a), with 200 pM TGF-β (PeproTech) dissolved in culture media for 4 d.

### CRISPR-Cas9–mediated *PANX2* deletion in REK cells
CRISPR/Cas9 technology was used to generate PANX2 KO REK cells (REK-PANX2KO) according to Synthego's nucleofection CRISPR protocol. The CRISPRevolution single-guide RNA (sgRNA) EZ kit targeting the beginning of exon 2 of rat *Panx2* gene (sequence: GCACAACUUCACCCGUGACC) and Cas9 2NLS nuclease were obtained from Synthego (Menlo Park, CA). One million cells/reaction were used for nucleofection with complexed ribonucleoprotein (9:1, sgRNA-to-Cas9 ratio) and Nucleofector solution L + supplement in a Nucleofector II (Amaxa Biosystems, Germany) according to the manufacturer's instructions. Expansion and clonal selection were then performed postnucleofection and genomic DNA isolated for genome sequencing and analysis by Inference of CRISPR Edits (Synthego). Platinum Taq DNA High Fidelity polymerase (Invitrogen; REF#11304-011; Carlsbad, CA) was used for PCR to genotype the target region as per the manufacturer instructions using the following primers: Px2-F (5'-GGGGGTTCATTTGGGGAACA-3') and Px2-R (5'-CAGGAAGTTGAGCTCGGAGG-3'). The genomic deletion was confirmed by Sanger sequencing provided by the London Regional Genomics Centre (Robarts Research Institute, London,ON, Canada).

## Mutagenesis of FLAG-tagged PANX2 constructs

The mouse *Panx2* (canonical) construct from Penuela *et al.* (2007) was used to fuse a single FLAG epitope (DYKDDDDK) to the N-terminal region of the PANX2 using the In-Fusion HD Cloning Kit protocol (Clontech, Mountain View, CA) as per the manufacturer's directions using the following primers: NFLAG sense (5′-ACCATGG ATTACAAGGACGACGATGACAAGGGTTCTTCCCACCACC-TCCTGGAGC-3′) and antisense (5′-GTCGTCCTTGTAATCCATGGT-GAATTCCACCACACTG-3′). The Procleave webserver (Li *et al.*, 2020) was used to predict the caspase cleavage consensus sites, and site-directed mutagenesis was performed by NorClone Biotech Labs (London, ON, Canada).

## Protein extractions and WBs

Cell lysates and co-IP assays were performed as described in Penuela *et al.* (2007, 2009). Total protein concentrations were quantified with the Pierce BCA Protein assay kit (Thermo Scientific; REF#23225; Rockford, IL). Protein lysates (40 µg) were resolved by 10% SDS–PAGE or TGX Stain-Free FastCast 10% Acrylamide stain-free gels (Cat#161-0183; Bio-Rad, USA) and transferred onto nitrocellulose membranes using an iBlot Blotting System (Invitrogen, USA). Membranes were blocked with 3% bovine fraction V heat shock serum albumin (BSA) (BioShop; REF# ALB001.100; Burlington, ON, Canada) in 0.05% Tween 20–phosphate-buffered saline (T-PBS) for 45 min and probed overnight at 4°C with the primary antibodies. Primary antibodies used for WBs anti–PANX2-CT-523 (Penuela *et al.*, 2009) (1:500 dilution); Anti-FLAG M2 monoclonal antibody (REF#F3165; Sigma-Aldrich, St. Louis, MO), anti–Panx2-NT (Cat#ARP42778_T100; Aviva Systems Biology, San Diego, CA) (Swayne *et al.*, 2010), mouse monoclonal anti-PANX2 (clone N121A/31 75-213) antibody (UC Davis/NIH NeuroMab Facility, Davis, CA) (Le Vasseur *et al.*, 2014), and cleaved caspase-3 (D175) (REF#9661S; Cell Signaling Technology, USA) were used at 1:1000 dilution; anti-GAPDH (Cat#MAB374, RRID: AB_2107445; Millipore, USA) was used at 1:5000 as the gel loading control. For detection, secondary antibodies IRDye -800CW and -680RD (LI-COR Biosciences, Lincoln, NE) were used at 1:25,000 dilution. WBs were visualized with the Odyssey infrared imaging system (LI-COR, USA) except for the skin lysates. For skin protein lysate immunoblots on nitrocellulose membranes, stain-free total protein was used for total protein determination imaged with a ChemiDoc MP System (Bio-Rad, USA). As an internal control to assess blot-to-blot variations, a brain lysate control was resolved on each gel and used for normalization. Normalization and densitometry measurements of bands of interest were done using Image Lab Software (Ver. 6.0.1; Bio-Rad Laboratories). Other densitometry and lane profile analyses for MW estimations of caspase-cleaved PANX2 fragments were performed using ODYSSEY application software (Ver. 3.0.16, LI-COR, USA).

## IF and imaging

Dorsal skin tissue samples were fixed in 10% neutral buffered Formalin overnight at 4°C, processed in the Molecular Pathology Core Facility at Robarts Research Institute (London, ON, Canada), and subsequently embedded in paraffin. Five-micrometer-thick sections were deparaffinized in xylene, rehydrated in graded alcohols, and washed in PBS. Antigen retrieval was performed using 1.5% of Vector Labs Tris-based Antigen Unmasking Solution (Cat#H-3301; Vector Labs, Burlingame, CA) heating for 5 min in a 750 W microwave (at 80% power) and then cooled down at room temperature (RT) for 10 min. Next, sections were rinsed once in distilled water, followed by PBS for 5 min. The sections were incubated with blocking solution (3% BSA, 0.1% Triton X-100 in 1× PBS) for 1 h at RT in a humidity

chamber. IF labeling of sections was performed overnight at 4°C with the primary antibodies diluted in blocking solution. Rabbit anti–PANX2 -CT, -IL, -NT polyclonal antibodies were used at ~100 µg/ml final concentration. Alexa Fluor 488 goat anti-rabbit IgG (Cat#A-11008; Thermo Fisher Scientific, USA) (2.9 µg/ml) was used as a secondary antibody. Slides were mounted using VECTASHIELD mounting medium (Vector Laboratories). For coverslip immunostaining, cell monolayers were washed with D-PBS (Life Technologies) and fixed with ice-cold methanol: acetone (5:1, vol/vol) for 15 min at 4°C. Coverslips were blocked for 1 h at RT with 10% normal goat serum (Life Technologies; REF#50062Z; Frederick, MD). Primary anti–PANX2-CT or anti-FLAG antibodies were used in 1:100 and 1:500 dilutions in 1% normal goat serum–2% BSA-PBS. Coverslips were incubated with primary antibodies for 1 h at RT and then washed with PBS and reincubated with donkey anti-mouse antibody Alexa Fluor 488 (1:400; Cat#A-21202; Invitrogen) and Texas Red-X goat anti-rabbit (diluted 1:500; REF#T6391; Life Technologies, Eugene, OR) to label FLAG-tagged PANX2. Aqua-Mount medium (Lerner Lab; REF#13800; USA) was used as mounting media. In all cases, Hoechst 33342 (REF#H3570; Life Technologies, Eugene, OR) (diluted 1:1000 in double-distilled water) was incubated with the samples for 7 min at RT to stain cell nuclei. Images were obtained on a Zeiss LSM 800 AiryScan confocal microscope from the Schulich Faculty Imaging Core Facility using the following objectives: LCI Plan-Neofluar 25×/0.8 1 mm Korr DIC for skin sections and Plan-Apochromat 63×/1.40 Oil DIC M27 for coverslips.

## Detection of caspase-cleaved PANX2 fragments

In vitro caspase-3 cleavage and IP of cleaved fragments were performed as described in Penuela *et al.* (2014b). For UVB-induced apoptosis assays, protein lysates from apoptotic cells were obtained after 8 h of post–UVB irradiation, and a similar IP (using 250 µg of total protein) was performed to capture the PANX2 cleaved fragments. Twenty-five micrograms of the input protein lysates was used for assessing protein expression by WB. In both cases (after caspase-3 treatment or in-cell UVB-induced apoptosis), the beads used for IP were dried by aspiration, resuspended in 2× Laemmli buffer (with β-mercaptoethanol), boiled for 5 min, and run in 10% SDS–PAGE gel for immunoblots with the anti-FLAG monoclonal antibody.

## RNA isolation and real-time qPCR

Total RNA was extracted from flash-frozen mouse dorsal skin samples at different ages using Ambion TRIzol Reagent (Life Technologies; REF#15596018; Carlsbad, CA) and purified using the RNAeasy Plus Mini kit (REF#74134; Qiagen GmbH, Hilden, Germany). For cell cultures, RNA was extracted with the RLT lysis buffer (Qiagen) and QIAshredder spin columns (REF# 79654; Qiagen GmbH, Hilden, Germany) instead of TRIzol. All protocols were used following the manufacturer's instructions. The RNA concentration was determined using an Epoch Microplate Spectrophotometer (BioTek, Winooski, VT). Reverse transcription (RT)-PCR was performed using the High Capacity cDNA Reverse Transcription Kit with RNase inhibitor (Applied Biosystems; REF#4374966; Thermo Fisher Scientific, Vilnius, Lithuania). A CFX96 Touch TM Real-Time PCR Detection System (Bio-Rad, Hercules, CA) and Sensifast SYBR Green PCR Master Mix (Cat#1725274; Bio-Rad, USA) were used to determine the mean quantitation cycle (Cq) for each sample in triplicate, and the relative transcript expression was calculated using the ΔΔCt method in Bio-Rad CFX Maestro Software, Ver. 1.1 (Bio-Rad, USA). In each case, mRNA expression was calculated relative to one of the samples of the undifferentiated group control. Log values were

used for statistical analyses, and geometric means were used for graphs. Primer sequences used for real-time qPCR are listed in Supplemental Table S1.

## UVB irradiation for induction of apoptosis

Forty-eight hours posttransfection REK-PANX2KO cells cultured in 60-mm plates were washed once with sterile Dulbecco-PBS (without $Ca^{2+}$ or $Mg^{2+}$) (Life Technologies; REF#14190-250). Cell monolayers kept in prewarmed D-PBS were placed 16 cm below a UVM-26 EL series, 8-W lamp (UVP, Upland, CA) and immediately subjected to lethal UVB treatment (302 nm, 1500 J/m²) or mock-irradiated. A UVB dosimeter was used to control the irradiance intensity. Then, culture media was immediately replaced, and cells were kept in the incubator until being harvested for protein lysates or cultured in the Incucyte Live-cell Imaging System for continuous cell death monitoring.

## Live-cell imaging of UVB-induced caspase-3 activation and cytotoxicity

Five thousand cells/well were seeded in a flat-bottom 96-well culture plate (Sarstedt; REF#83.3924; Nümbrecht, Germany) with MEM (Life Technologies; Cat#11095-080; Grand Island, NY) culture media supplemented with 10% FBS and 1% Pen Strep antibiotics. Cells were allowed to attach to the bottom of the plate for 30 min in the incubator before being monitored. After UVB treatment, prewarmed MEM culture media was added, supplemented with IncuCyte Caspase-3/7 Green Apoptosis Reagent (Sartorius; Cat# 4440; USA) at 1/1000 dilution and Cytotox Red Reagent (Sartorius; Cat#4632; USA) at 250 nM final concentration. Live-cell images were acquired with a 10× objective every 2 h for 50 h, with phase, green, and red channels using an IncuCyte S3 Live-Cell Analysis System (Essen Bio-Science, Ann Arbor, MI). Acquired data were analyzed using the Cell-by-cell Analysis Module in the IncuCyte 2020A Software package (Essen BioScience, USA).

## Transfection efficiency determination and IncuCyte data analysis

The fold change (from phase or fluorescence data) over time was calculated by dividing the object counts (determined by Cell-by-cell Analysis) of any given time point by the counts acquired at the beginning of the experiment (i.e., 0 h). To account for transfection efficiency, the fold change was divided by a normalization factor (Nf) calculated as per Eq. 1:

$$Nf = 1 + TE \qquad (1)$$

TE corresponds to the transfection efficiency, and nontransfected cells were arbitrarily set as TE = 0 (e.g., Nf = 1 if cells are untransfected). TE was estimated by the percentage of cells positive for PANX2(FLAG) IF grown in coverslips and fixed at the start of apoptosis experiments. Counts were done by automatic quantification using Cell Profiler Software (Ver. 4.0.7; Broad Institute, USA) (Lamprecht *et al.*, 2007) using at least 50 nonoverlapping IF images per field. In this case, IF images were acquired with a Ni-E Fluorescence Microscope (Nikon, Japan) using an S Plan Fluor ELWD 20× Ph1 ADM 0.45 N/A objective. Normalized data are shown in time-course graphs after adjusting the range of values from 0% (first measurement) to 100% (last acquired value) using GraphPad Prism software (Ver. 8.0). For the estimation of the time to apoptosis, normalized data were fitted to an allosteric sigmoidal function (Eq. 2):

$$\%Cact = \frac{Cmax \times t^a}{t50\%^a + t^a} \qquad (2)$$

where %Cact corresponds to the percent of caspase activation (Cact) at any given time ($t$); Cmax is the caspase activation when ~100% of the cells are apoptotic and caspase-3/7 signal is saturated, $t_{50\%}$ is the time to reach half-maximal caspase activation (~50% of cells are apoptotic), and $a$ is the slope factor in the curve. Only accurate curve fitting was used for the estimations considered when the goodness of fit ($R^2$) ≥ 0.95.

## Statistical analysis

Unless otherwise indicated, all data are presented as the mean ± standard error of the mean (SEM) and represent at least three independent biological replicates or experiments ($N$ = 3) conducted with at least two technical replicates ($n$ = 2). Statistical analyses are indicated in the figure captions and were performed using GraphPad Prism software (Ver. 8.0) (La Jolla, CA).

## REFERENCES

Abitbol JM, O'Donnell BL, Wakefield CB, Jewlal E, Kelly JJ, Barr K, Willmore KE, Allman BL, Penuela S (2019). Double deletion of Panx1 and Panx3 affects skin and bone but not hearing. J Mol Med (Berl) 97, 723–736.

Aken BL, Ayling S, Barrell D, Clarke L, Curwen V, Fairley S, Fernandez Banet J, Billis K, Garcia Giron C, Hourlier T, *et al.* (2016). The Ensembl gene annotation system. Database (Oxford) 2016, baw093.

Baden HP, Kubilus J (1983). The growth and differentiation of cultured newborn rat keratinocytes. J Invest Dermatol 80, 124–130.

Baranova A, Ivanov D, Petrash N, Pestova A, Skoblov M, Kelmanson I, Shagin D, Nazarenko S, Geraymovych E, Litvin O, *et al.* (2004). The mammalian pannexin family is homologous to the invertebrate innexin gap junction proteins. Genomics 83, 706–716.

Bargiotas P, Krenz A, Hormuzdi SG, Ridder DA, Herb A, Barakat W, Penuela S, von Engelhardt J, Monyer H, Schwaninger M (2011). Pannexins in ischemia-induced neurodegeneration. Proc Natl Acad Sci USA 108, 20772–20777.

Bargiotas P, Krenz A, Monyer H, Schwaninger M (2012). Functional outcome of pannexin-deficient mice after cerebral ischemia. Channels (Austin) 6, 453–456.

Berchtold LA, Miani M, Diep TA, Madsen AN, Cigliola V, Colli M, Krivokapic JM, Pociot F, Eizirik DL, Meda P, *et al.* (2017). Pannexin-2-deficiency sensitizes pancreatic beta-cells to cytokine-induced apoptosis in vitro and impairs glucose tolerance in vivo. Mol Cell Endocrinol 448, 108–121.

Borowiec AS, Delcourt P, Dewailly E, Bidaux G (2013). Optimal differentiation of in vitro keratinocytes requires multifactorial external control. PLoS One 8, e77507.

Bruzzone R, Hormuzdi SG, Barbe MT, Herb A, Monyer H (2003). Pannexins, a family of gap junction proteins expressed in brain. Proc Natl Acad Sci USA 100 13644–13649.

Candi E, Knight RA, Panatta E, Smirnov A, Melino G (2016). Cornification of the skin: a non-apoptotic cell death mechanism. eLS, a0021583.pub2, 1–10.

Celetti SJ, Cowan KN, Penuela S, Shao Q, Churko J, Laird DW (2010). Implications of pannexin 1 and pannexin 3 for keratinocyte differentiation. J Cell Sci 123, 1363–1372.

Chekeni FB, Elliott MR, Sandilos JK, Walk SF, Kinchen JM, Lazarowski ER, Armstrong AJ, Penuela S, Laird DW, Salvesen GS, *et al.* (2010). Pannexin 1 channels mediate "find-me" signal release and membrane permeability during apoptosis. Nature 467, 863–867.

Cowan KN, Langlois S, Penuela S, Cowan BJ, Laird DW (2012). Pannexin1 and Pannexin3 exhibit distinct localization patterns in human skin appendages and are regulated during keratinocyte differentiation and carcinogenesis. Cell Commun Adhes 19, 45–53.

Dickinson ME, Flenniken AM, Ji X, Teboul L, Wong MD, White JK, Meehan TF, Weninger WJ, Westerberg H, Adissu H, *et al.* (2016). High-throughput discovery of novel developmental phenotypes. Nature 537, 508–514.

Engelhardt K, Schmidt M, Tenbusch M, Dermietzel R (2015). Effects on channel properties and induction of cell death induced by c-terminal truncations of pannexin1 depend on domain length. J Membr Biol 248, 285–294.

Lai CP, Bechberger JF, Naus CC (2009). Pannexin2 as a novel growth regulator in C6 glioma cells. Oncogene 28, 4402–4408.

Lamprecht MR, Sabatini DM, Carpenter AE (2007). CellProfiler: free, versatile software for automated biological image analysis. Biotechniques 42, 71–75.

Le Vasseur M, Chen VC, Huang K, Vogl WA, Naus CC (2019). Pannexin 2 localizes at ER-mitochondria contact sites. Cancers (Basel) 11, 343.

Le Vasseur M, Lelowski J, Bechberger JF, Sin WC, Naus CC (2014). Pannexin 2 protein expression is not restricted to the CNS. Front Cell Neurosci 8, 392.

Li D, Turi TG, Schuck A, Freedberg IM, Khitrov G, Blumenberg M (2001). Rays and arrays: the transcriptional program in the response of human epidermal keratinocytes to UVB illumination. FASEB J 15, 2533–2535.

Li F, Leier A, Liu Q, Wang Y, Xiang D, Akutsu T, Webb GI, Smith AI, Marquez-Lago T, Li J, Song J (2020). Procleave: predicting protease-specific substrate cleavage sites by combining sequence and structural information. Genom Proteom Bioinform 18, 52–64.

Liao D, Yang G, Yang Y, Tang X, Huang H, Shao J, Pan Q (2020). Identification of Pannexin 2 as a novel marker correlating with ferroptosis and malignant phenotypes of prostate cancer cells. Onco Targets Ther 13, 4411–4421.

Lippens S, Denecker G, Ovaere P, Vandenabeele P, Declercq W (2005). Death penalty for keratinocytes: apoptosis versus cornification. Cell Death Differ 12(Suppl 2), 1497–1508.

Maher AC, Thomas T, Riley JL, Veitch G, Shao Q, Laird DW (2005). Rat epidermal keratinocytes as an organotypic model for examining the role of Cx43 and Cx26 in skin differentiation. Cell Commun Adhes 12, 219–230.

Panchin Y, Kelmanson I, Matz M, Lukyanov K, Usman N, Lukyanov S (2000). A ubiquitous family of putative gap junction molecules. Curr Biol 10, R473–R474.

Penuela S, Bhalla R, Gong XQ, Cowan KN, Celetti SJ, Cowan BJ, Bai D, Shao Q, Laird DW (2007). Pannexin 1 and pannexin 3 are glycoproteins that exhibit many distinct characteristics from the connexin family of gap junction proteins. J Cell Sci 120, 3772–3783.

Penuela S, Bhalla R, Nag K, Laird DW (2009). Glycosylation regulates pannexin intermixing and cellular localization. Mol Biol Cell 20, 4313–4323.

Penuela S, Gehi R, Laird DW (2013). The biochemistry and function of pannexin channels. Biochim Biophys Acta 1828, 15–22.

Penuela S, Kelly JJ, Churko JM, Barr KJ, Berger AC, Laird DW (2014a). Panx1 regulates cellular properties of keratinocytes and dermal fibroblasts in skin development and wound healing. J Invest Dermatol 134, 2026–2035.

Penuela S, Lohman AW, Lai W, Gyenis L, Litchfield DW, Isakson BE, Laird DW (2014b). Diverse post-translational modifications of the pannexin family of channel-forming proteins. Channels (Austin) 8, 124–130.

Sanchez-Pupo RE, Johnston D, Penuela S (2018). N-glycosylation regulates Pannexin 2 localization but is not required for interacting with Pannexin 1. Int J Mol Sci 19, 1837.

Sandilos JK, Chiu YH, Chekeni FB, Armstrong AJ, Walk SF, Ravichandran KS, Bayliss DA (2012). Pannexin 1, an ATP release channel, is activated by caspase cleavage of its pore-associated C-terminal autoinhibitory region. J Biol Chem 287 11303–11311.

Scemes E, Veliskova J (2019). Exciting and not so exciting roles of pannexins. Neurosci Lett 695, 25–31.

Swayne LA, Sorbara CD, Bennett SA (2010). Pannexin 2 is expressed by postnatal hippocampal neural progenitors and modulates neuronal commitment. J Biol Chem 285, 24977–24986.

Wang XH, Streeter M, Liu YP, Zhao HB (2009). Identification and characterization of pannexin expression in the mammalian cochlea. J Comp Neurol 512, 336–346.

Wicki-Stordeur LE, Boyce AK, Swayne LA (2013). Analysis of a pannexin 2-pannexin 1 chimeric protein supports divergent roles for pannexin C-termini in cellular localization. Cell Commun Adhes 20, 73–79.

Xu X, Hao Y, Xiong S, He Z (2021). PANX2 and brain lower grade glioma genesis: a bioinformatic analysis. Sci Prog 104, 368504211011836.

Zhang P, Ishikawa M, Doyle A, Nakamura T, He B, Yamada Y (2021). Pannexin 3 regulates skin development via Epiprofin. Sci Rep 11, 1779.

Zhang P, Ishikawa M, Rhodes C, Doyle A, Ikeuchi T, Nakamura K, Chiba Y, He B, Yamada Y (2019). Pannexin-3 deficiency delays skin wound healing in mice due to defects in channel functionality. J Invest Dermatol 139, 909–918.